On the Design of a Microwave Imaging System to Monitor Thermal Ablation of Liver Tumors

Mengchu Wang, *Student Member, IEEE*, Lorenzo Crocco, *Senior Member, IEEE*, and Marta Cavagnaro, *Member, IEEE*

***Abstract*—Thermal ablation treatment of cancer is increasingly adopted in the clinical practice, being minimally invasive and highly specific. However, a significant drawback of the technique is the lack of effective imaging modalities for monitoring the changes undergoing in the thermally treated tissue. In this respect, microwave imaging has been proposed as a possible candidate, owing to its portability, low-cost, non-ionizing nature, and capability to detect changes in dielectric properties of tissues induced by the temperature. The goal of this paper is to provide the guidelines for the design of a microwave imaging system for thermal ablation monitoring of liver tumors. To this end, an analytical study is performed to determine the proper working conditions, in terms of frequency band and matching medium. Then, three antipodal Vivaldi antennas on different dielectric substrates are designed and numerically assessed. Among those antennas, the Vivaldi antenna on RT/duroid 6010LM substrate proved to be the most suitable choice. The results of this study pave the way to an experimental assessment of microwave imaging as a modality to monitor thermal ablation treatments.**

***Index Terms*—Electromagnetic devices, microwave imaging, thermal ablation, ultra wideband antennas, vivaldi antennas.**

I. Introduction

LIVER cancer is recognized as a disease with an increased death rate every year [1]. Indeed, in the last 40 years, the overall death rate has doubled its number [1]. To improve the survival rate, the success of early-stage diagnoses and following clinical treatments is fundamental [2].

Microwave thermal ablation (MTA) is a treatment that destroys the tumor with a minimally invasive approach [3]. Clinical studies demonstrated that it has a good effect on small (less than 3 cm) to medium size lesions (3–5 cm) [4]. However, remotely monitoring the ablation region during the treatment and detection of the ablation temperature remain distinct tasks for researchers [5].

Several imaging modalities have been used in the clinical settings. Ultrasound (US) shows attractive characteristics as it provides real-time imaging and is cost-effective [6]. However, when it comes to thermal ablation of tissue with large water content such as the liver, the US sensor is blinded by a hyperechogenic cloud caused by water vaporization [7]. Magnetic resonance imaging (MRI) can provide high-resolution temperature maps [5]. Currently, it is the only modality with well validated techniques for real time temperature monitoring [8]. However, its bulky size and high cost are constraints for cost-effective systems [5]. Additionally, compatibility issues are present between MRI and MTA devices [9]. Finally, computed tomography scan (CT) can monitor temperature during ablation treatments [10]. However, high dose ionizing radiation caused by multiple scans during the treatment could cause DNA mutations [11]. Therefore, CT is not suitable for long time exposures and is more often used for clinical follow-up [12].

In comparison with the imaging modalities mentioned above, microwave imaging (MWI) shows characteristics able to overcome all cited difficulties, being harmless, compact-sized and low-cost [13]. The principle of MWI is based on processing the electromagnetic (EM) field scattered by the body to create images of the dielectric properties of tissues [13]. Given the significant changes that electric properties of tissue undergo during ablation treatments [14], MWI is viable for monitoring the progresses during the procedures [15]. Most of biomedical applications of MWI operate in the ISM band, particularly around 2.45 GHz [13], [16].

A first experimental proof of the applicability of MWI for monitoring thermal ablation was given in [15], where an imaging experiment was performed on an *ex vivo* liver sample probed before and after an 8-minute long treatment. However, while providing a confirmation of the potential of MWI, such a study was based on a set-up not specifically designed for the application at hand. In particular, both used antipodal antennas (a heart-shaped one [17] and a Vivaldi one [18]) had been designed for UWB radar applications in the frequency band from 3 to 10 GHz. As it will be shown later on in the manuscript, MWI systems perform better using frequencies below 2 GHz. Indeed, given the encouraging results in [15], antennas specifically designed for the foreseen system are now needed.

Starting from the positive outcomes of [15], in this paper the design of an ad-hoc MWI thermal ablation monitoring system

Manuscript received July 20, 2020; revised October 2, 2020 and December 8, 2020; accepted December 24, 2020. Date of publication January 1, 2021; date of current version August 21, 2021. This work was supported by the EMERALD project funded by the European Union's Horizon 2020 Research and Innovation Program under the Marie Skłodowska-Curie Grant 764479. *(Corresponding author: Mengchu Wang.)*

Mengchu Wang is with the CNR-IREA, National Research Council of Italy Institute for Electromagnetic Sensing of the Environment, Napoli 80124, Italy, and also with the Department of Information Engineering, Electronics, and Telecommunications, University of Rome "La Sapienza", 00184 Rome, Italy (e-mail: wang.m@irea.cnr.it).

Lorenzo Crocco is with the CNR-IREA, National Research Council of Italy Institute for Electromagnetic Sensing of the Environment, Napoli 80124, Italy (e-mail: crocco.l@irea.cnr.it).

Marta Cavagnaro is with the Department of Information Engineering, Electronics, and Telecommunications, University of Rome "La Sapienza", 00184 Rome, Italy, and also with the CNR-IREA National Research Council of Italy Institute for Electromagnetic Sensing of the Environment, Napoli 80124, Italy (e-mail: marta.cavagnaro@uniroma1.it).

Digital Object Identifier 10.1109/JERM.2020.3048846

was faced. In particular in this contribution, first, the optimal working conditions are determined in terms of frequency band and properties of the medium to be adopted for improving the matching between the probing field and the human body. To this end, a 1-D 4-layered abdomen region was studied and the transmission coefficient as a function of the frequency and external medium was evaluated. This approach already proved successful to study this kind of problems (e.g. brain MWI [19]). Then, the results achieved with the 1-D model are verified studying a cylindrical geometry. Finally, the design and numerical characterization of a compact Vivaldi antenna to be used in the imaging experiments is presented. Vivaldi antennas are typically used for medical imaging applications thanks to their end-fire radiation pattern which allows high density array arrangement [20]. Besides, Vivaldi antennas can easily achieve wideband performances without complex bandwidth enhancement designs [21]. The Vivaldi antenna proposed in this paper is simulated in the suggested matching medium; it shows a bandwidth from 500 MHz to 5 GHz. An investigation of different antenna substrates was carried out aiming for antenna's miniaturization. Finally, SMA feedings problems inside the matching medium were put into evidence and a possible solution was proposed.

II. Materials and Methods

A. Simplified Models

In an MWI system, the antennas are usually located within a medium that matches the EM field radiated by the antenna to the biological tissues [22]. Accordingly, in this paper the matching medium properties and the antennas' frequency band are chosen such that the largest possible portion of the EM power enters the abdomen and provides a meaningful backscattered signal after interacting with the liver [19]. To this end, as a first-order approximation, the region of interest can be represented by a semi-infinite multi-layer planar slab, composed of skin, fat, muscle, and liver. Similarly, the EM field propagating within the matching medium and impinging on the layered model can be represented by way of a plane wave traveling in a direction orthogonal to the interface between the medium and the skin. Based on average statistics, the thickness of the skin was taken equal to 2.3 mm, that of fat 12.2 mm, and that of muscle 20.2 mm [23], [24]. The last layer, mimicking the liver, is considered to be semi-infinite in-depth, being the target of the analysis. The frequency dependent dielectric properties of the different tissues were modeled as a single pole Cole-Cole model whose parameters were taken from [25].

The above described structure can be studied using the transmission line (TL) formalism [26], see Figure 1. Following the TL equivalence, the characteristic impedance of the line segment corresponding to the n-th tissue is given as [26]:

$$Z_n = \sqrt{\mu_0/\varepsilon_0\varepsilon_n} \tag{1}$$

where ε_n is the complex relative permittivity of the n-th tissue. In the following, Z_{mm}, Z_s, Z_f, Z_m and Z_l denote the characteristic impedances of matching medium, skin, fat, muscle, and liver, respectively. According to the impedance transfer equation, the equivalent impedance at interface CC' (Figure 1) between fat and muscle is [26]:

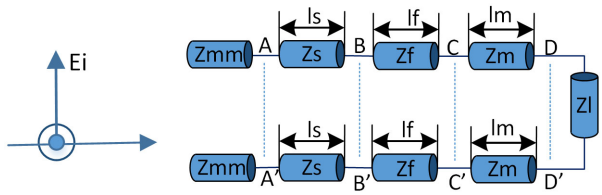

Fig. 1. Transmission line model of a plane wave impinging orthogonally on a planar layered structure.

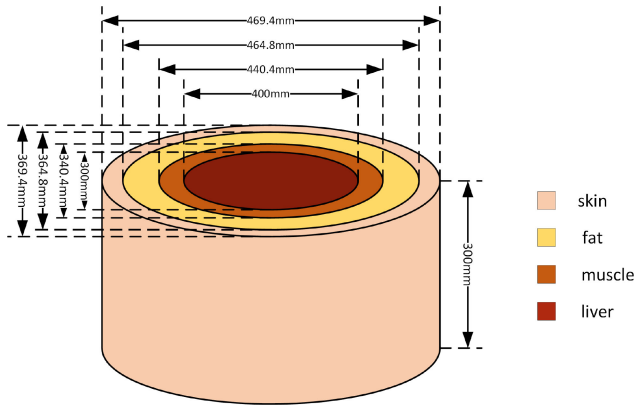

Fig. 2. Cylindrical geometry.

$$Z_{CC'} = Z_m \cdot \frac{Z_{DD'} + jZ_m \cdot \tan k_m l_m}{Z_m + jZ_{DD'} \cdot \tan k_m l_m}, \tag{2}$$

where $Z_{DD'} = Z_l$ represents the impedance of the liver. The equivalent impedance at interface BB' between skin and fat is calculated with an equation readily obtained from 2, by simply replacing Z_m with Z_f, l_m with l_f, and $Z_{DD'}$ with $Z_{CC'}$, respectively. The equivalent impedance at interface AA' between matching medium and the skin is computed in the same way. Finally, from the knowledge of $Z_{AA'}$, the reflection coefficient of the electric field at the interface between the matching medium and skin can be evaluated as:

$$\Gamma_{AA'} = \frac{Z_{AA'} - Z_{mm}}{Z_{AA'} + Z_{mm}} \tag{3}$$

while the power transmission coefficient at the interface is:

$$T_{AA'} = 1 - |\Gamma_{AA'}|^2 . \tag{4}$$

To verify the results achieved with the TL model, a 3D cylindrical layered structure with elliptical cross-section mimicking the abdomen was considered. The detailed geometry is given in Figure 2.

B. Antipodal Vivaldi Antenna (AVA)

In MWI, the imaging resolution can be improved by increasing the number of antennas [27]. Hence, it is preferable to use compact antennas to allow a larger number of elements to be used. Several substrates were considered in this study to design an antenna as small as possible. In particular, RT/duriod 6010LM (Rogers Cooperation, USA, $\varepsilon_{sub} = 10.2$), T-Ceram E-20 material (T-Ceram, S.r.o. Czechia, $\varepsilon_{sub} = 20.0$), and T-Ceram E-37 (T-Ceram, S.r.o. Czechia, $\varepsilon_{sub} = 37$) were considered.

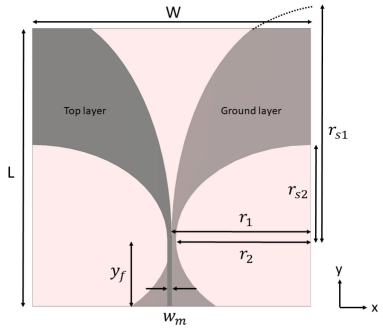

Fig. 3. Antipodal Vivaldi Antenna (AVA) geometry, W=60 mm, L=60 mm, $w_m = 0.9$ mm, $y_f = 14.5$ mm, $r_1 = 30$ mm, $r_2 = 29.1$ mm, $r_{s1} = 50.1$ mm, $r_{s2} = 20.37$ mm (gray: metallic layer, pink: substrate).

The thicknesses of these antenna substrates are 1.905 mm, 2 mm, and 2 mm respectively, plus a 17-μm-thick conductive coating. The antipodal Vivaldi antenna with RT/duriod 6010LM substrate (AVA-RT) (Figure 3) and the antipodal Vivaldi antenna with T-Ceram E-20 substrate (AVA-E-20) were designed by following [28], where an antenna working in the 3-10 GHz band is presented. The antipodal Vivaldi antenna with T-Ceram E-37 substrate (AVA-E-37) was designed applying equation (1) in [29]. Such antennas were chosen for their compact size and because they were designed for imaging purposes [28], [29]. The design study was then aimed at taking the advantageous features of those antennas and translating them into the considered scenario, wherein the antenna is immersed in the matching medium (not in air). In particular, the matching medium reduces the wavelength of a factor $1/\sqrt{\varepsilon_m}$ (ε_m is the relative permittivity of the material), with respect to air. Therefore, it allows reducing antenna's dimensions preserving its working capabilities at lower frequencies (i.e. below 1 GHz).

C. EM Modeling Software and Simulations

The study of the plane wave impinging on the cylindrical geometry shown in Figure 2 was carried out using WIPL-D Pro CAD (WIPL-D d.o.o., Serbia) [30], which is an EM simulation software, based on the methods of moments. All antennas were designed and simulated through CST software (Dassault Systèmes, France). CST is a software based on the finite integration technique applied to Maxwell's curl equation in the time domain. It is a marching in time procedure that simulates the propagation and interaction of EM waves in a region of space [31]. The antennas were fed by waveguide feedings looking for the best matching in the frequency band derived from the numerical study described in section II-A. To achieve this goal, the parameter sweep function of the CST software was applied for W ($W_{min} = 50$ mm, $W_{max} = 70$ mm), L ($L_{min} = 50$ mm, $L_{max} = 70$ mm), w_m ($w_{mmin} = 0.7$ mm, $w_{mmax} = 1.2$ mm), antenna major ellipses radii r_{s1} ($r_{s1min} = 45$ mm, $r_{s1max} = 60$ mm) and minor ellipses radii r_{s2} ($r_{s2min} = 11$ mm, $r_{s2max} = 29$ mm), one at a time, with 10% sweep steps which were accordingly adjusted each time until the best antenna matching was achieved (see Figure 3). Firstly, a coarser sweep step was selected; if a better matching was achieved at a certain point, a finer step was used for a second sweep around this value. The simulation process was stopped when the results variations were less than 10%.

III. Result and Discussion

A. 1-D Transmission Line Model

Based on the formulas in Section II-A, the transmission coefficient at the interface between a generic lossless medium, with relative permittivity varying between 1 and 80, and the layered structure providing a simplified model of the abdomen was calculated in a frequency range between 500 MHz and 5 GHz. Figure 4(a) shows the calculated transmission coefficient as a function of the matching medium permittivity and frequency. The plot shows that, similar to what happens in other biomedical MWI applications [19], a 'forbidden transmission band' occurs from 2 GHz to 3 GHz, where the transmission coefficient is lower than 0.5. Such an effect arises because the layered structure is made by a low permittivity layer (fat), enclosed between two higher permittivity layers (skin and muscle, respectively), behaving like a waveguide at some frequencies [32]. Accordingly, less power is delivered to the target between 2 GHz and 3 GHz as compared to other portions of the frequency spectrum. The power transmission increases again above 3 GHz. However, the penetration depth of the EM wave severely decreases at higher frequencies, thus making difficult if not impossible to accurately measure useful signals. Accordingly, in the MWI system under design, it is preferable to use frequencies below 2 GHz. Following these considerations, Figure 4(a) suggests that the best choice would be a frequency band of 500 MHz–2 GHz and a matching medium with a permittivity value close to 23. In fact, although lower permittivity values show better transmission at lower frequencies, the 2–3.5 GHz stopband shows almost no power transmission to the target. On the contrary, higher permittivity values show degraded performances at the lower frequencies.

To verify if the unavoidable presence of losses has an effect on the previous outcomes, the transmission coefficient has been recomputed considering a matching medium with losses. In particular, the losses associated to a realistic medium obtained with a water-oil emulsion and showing a permittivity of about 23 at 915 MHz [33] were considered. Accordingly, the 1-D analysis was repeated considering a matching medium with relative permittivity between 1 and 80 and a conductivity of 0.07 S/m. As can be seen from Figure 4(b) the above findings are confirmed.

Finally, the transmission coefficient was computed when a layer of ablated tissue is present. To this end, a 6-layered structure made by skin, fat, muscle, liver, ablated zone, and liver was modeled. The thickness of the liver layer between muscle and ablated zone was set to 10 mm, and that of the ablated zone was 25 mm. The other tissue layers were the same as the pre-ablation model and the same matching medium was used. The dielectric properties of the thermally ablated liver were obtained from measurements done on a post-ablation *ex vivo* ovine liver [34].

The results are shown in Figure 4(c). As can be seen, the transmission coefficients in the two scenarios exhibit a similar behavior, confirming that the designed matching medium works properly, also in presence of the ablated tissue. In particular,

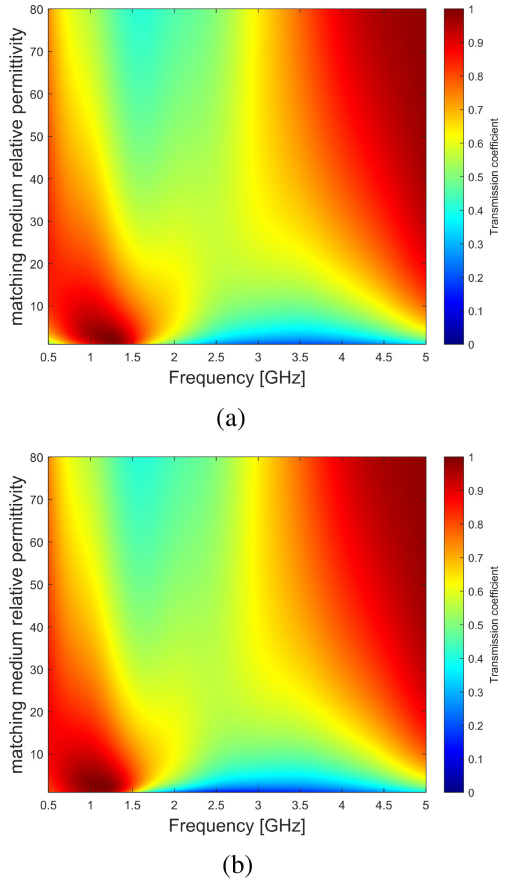

Fig. 4. Power transmission coefficient for different matching media: (a) lossless matching medium, (b) matching medium with conductivity 0.07 S/m, and (c)1-D transmission coefficient for a medium $\epsilon_r = 23$, $\sigma = 0.07$ S/m comparing healthy liver or liver with a thermally ablated area 2.5 cm thick.

above 2 GHz, the two curves are almost overlapping, in agreement with the effect of the foreseen stopband and the significant reduction of the penetration depth of the EM field at higher frequencies. In addition, at lower frequencies (below 2 GHz, which is the frequency range of interest), the two curves are clearly different. Although such a plot can give only a qualitative indication, it can be noted that the relative variation of the transmitted power due to the presence of the ablated tissue (expressed in dB and normalized to the power transmitted in the healthy liver) is in the order of -30 dB, This value is well

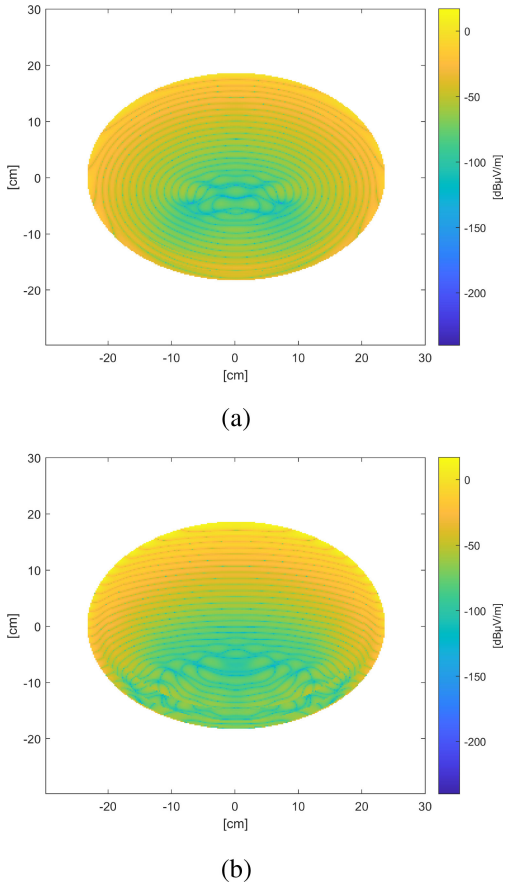

Fig. 5. E-Field distribution within a cylindrical layered phantom evaluated through WIPL-D at 1 GHz (a) phantom in free space and (b) phantom in matching medium with permittivity value of 23.

above the typical noise floor of standard VNAs, thus giving an indirect confirmation of the viability of the imaging concept preliminary demonstrated in [15].

B. EM Simulation Results in WIPL-D Environment

To verify the outcome of the 1-D analysis, a WIPL-D Pro simulation was carried out [30]. In particular, a plane wave impinging on a cylindrical layered structure mimicking the abdomen was simulated. The electric field amplitude was set to 1 V/m, and the electric field polarization was parallel to the axis of the cylinder.

Figure 5 shows the E-field distribution (unit: dB μV/m) in the central transversal section of the phantom, with respect to the height. In particular, Figure 5(a) is obtained considering the phantom surrounded by air, while Figure 5(b) refers the case in which the phantom is surrounded by a lossless matching medium with a relative permittivity value of 23. Plots have been normalized to the maximum E-field value in correspondence of the surface of the skin. Table I reports the maximum E-field absolute values at 1 GHz in the different tissues in the two cases, normalized to the maximum value recorded in the skin in the case of air surrounding the model. From Figure 5 and Table I, it can be noticed that the field values absorbed into the phantom when the matching medium is present are greater than when air is present. The results also confirm that E-field penetration

TABLE I
MAXIMUM E-FIELD NORMALIZED ABSOLUTE VALUE IN DIFFERENT TISSUE OF THE LAYERED CYLINDER AT 1 GHz

Maximum E-field normalized value (dBμV/m)		
	In air	In matching medium
Skin	0	32.0645
Fat	-3.8641	28.0761
Muscle	-31.1005	-1.273
Liver	-46.8066	-17.9472

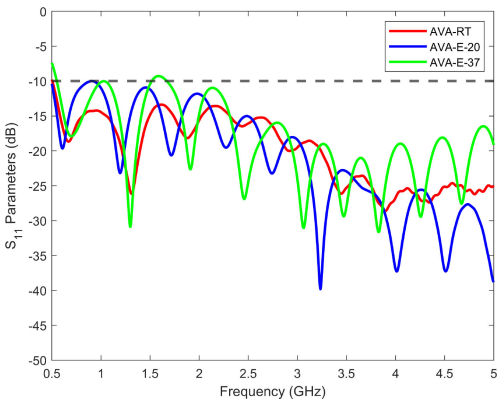

Fig. 6. Simulated S_{11} parameters of Vivaldi antennas on three different substrates: RT/duriod 6010LM, T-Ceram E-20, T-Ceram E-37. The antennas are immersed in a matching medium ($\epsilon_r = 23$, $\sigma = 0.07$ S/m).

TABLE II
DIMENSIONS OF VIVALDI ANTENNAS ON THREE DIFFERENT SUBSTRATES: RT/DUROID 6010 LM, T-CERAM E-20, T-CERAM E-37

Antenna Parameters [mm]			
	AVA-RT	AVA-E-20	AVA-E-37
W	60	60	42
L	60	60	50
W×L	3600	3600	2100
w_m	0.9	0.34	0.15
t_s	1.905	2	2

is frequency sensitive, as expected, and the considerations on the lower expected spatial resolution achievable when the air surrounds the geometry. Finally, it is worth noting that field coverage looks wider when air is present, in agreement with predictions derived from Figure 5(b). This is possibly due to surface waves traveling around the cylinder. However, this phenomenon is not desirable since it could give rise to scattered fields with arbitrary phase with respect the useful signal from the inside of the body. Accordingly, the reported results confirm that the use of the identified matching medium is the most suitable choice.

C. Antennas Design and Matching

As illustrated in Section II-B, three antipodal Vivaldi antennas were designed on three different substrates. The S_{11}-parameters of the antennas when operated in the matching medium are shown in Figure 6. The antennas cover a frequency band from 500 MHz to 5 GHz, which is more than the required bandwidth (500 MHz–2 GHz). Table II gives the dimensions of the antennas

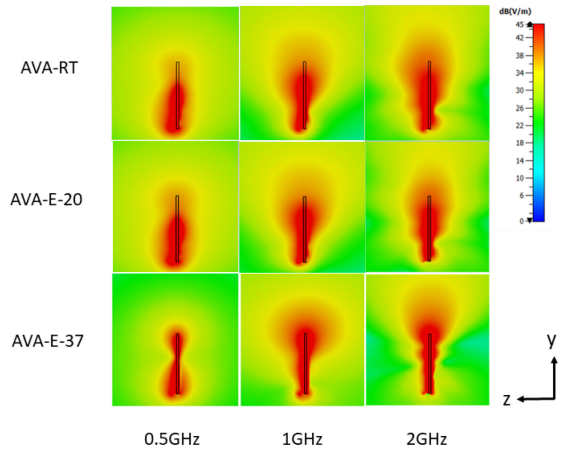

Fig. 7. E-field distribution of Vivaldi antennas on three different substrates: RT/duriod 6010LM, T-Ceram E-20, T-Ceram E-37. The antennas are immersed in a matching medium ($\epsilon_r = 23$, $\sigma = 0.07$ S/m).

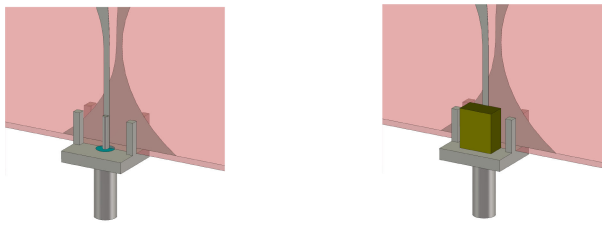

Fig. 8. Antenna feedings: (a) SMA connector and (b) SMA connector whose pin covered with epoxy resin.

after the optimization process. It is found that the antenna with RT/duriod 6010LM and the one with T-Ceram E-20 substrate are of the same dimension. Even if the permittivity value of the substrate material is higher, it does not successfully miniaturize the antenna dimension inside the matching medium. AVA-E-37 has the most compact dimension as compared to the other two antennas, with a 41% reduction. The E-field distributions on the yz plane (see reference system in Figure 3) of the optimized antennas inside the matching medium are shown in Figure 7, at 500 MHz, 1 GHz and 2 GHz. From the figure it is obvious that they exhibit similar behaviors.

In Section III-C, the antennas were simulated in CST with a waveguide feeding in order to simplify the model. In practice, the antenna is fed by a coaxial cable through an SMA connector. As known, the transition from a coaxial feeding to a microstrip line feeding could cause mismatch and introduce noise [35]. To characterize this behavior the three antennas in the previous section were considered with a coaxial feeding, as shown in Figure 8(a). Figure 9 shows the corresponding S_{11} parameters of the three antennas (dashed lines). As can be seen, when the antennas are connected to an SMA connector and placed inside the matching medium, all the antennas become mismatched. This is because the SMA connector is designed to work in air. To overcome this problem, a simple solution was proposed by covering the connector pin with an epoxy resin of permittivity equal to 4 and dimensions of $4.76 \times 5.75 \times 2.77$ mm^3 (see Figure 8(b)). This method could isolate the connector pin from the matching medium, thus avoiding the connector impedance

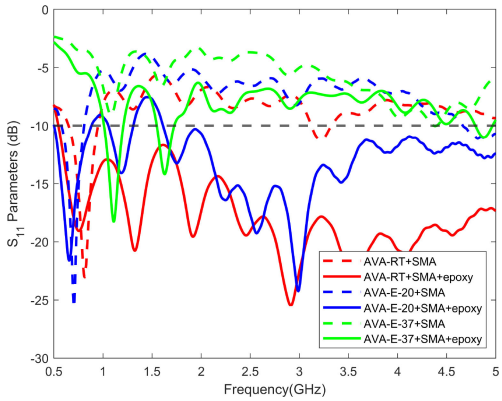

Fig. 9. Simulated S_{11} parameters of the three antennas with different feedings.

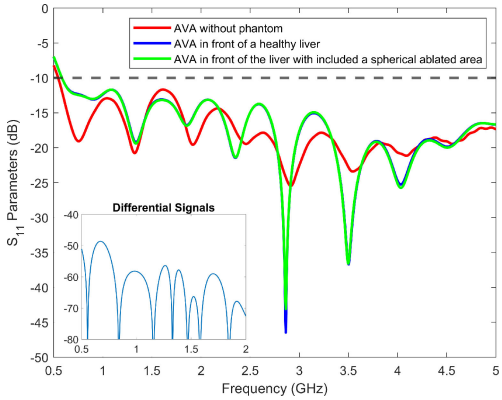

Fig. 10. Simulated S_{11} parameters of the AVA-RT antenna fed by SMA connector and immersed in the matching medium ($\epsilon_r = 23$, $\sigma = 0.07$ S/m) when the antenna radiates in the matching medium and when it is positioned in front of different abdomen phantoms.

mismatch. From the results in Figure 9 it can be noted that the use of the epoxy resin provides the expected effect for the AVA-RT antenna. Conversely, the AVA-E-20 antenna remains mismatched in the frequency range of interest (from 800 MHz to 1.8 GHz), and the AVA-E-37 remains mismatched throughout the whole frequency band. This is due to the large dielectric property difference between the substrate material and the epoxy resin. A sensitivity study was carried out with a slight variation of 1-2 mm of the epoxy resin dimension, however, the S_{11}-parameters of the antennas was barely changed.

D. AVA Behaviors in Realistic Conditions

Finally, simulations were carried out to verify the antenna behavior in the presence of the human body. To this end, the AVA-RT, fed by a SMA connector and immersed in the matching medium ($\epsilon_r = 23$, $\sigma = 0.07$ S/m) was placed in contact to a 4-layer abdomen phantom made by the same tissues, with the same thicknesses, as in Section II-A. Figure 10 compares the antenna's matching in the presence and in the absence of the phantom. From the figure it can be derived that the antenna keeps the matching when the human body is present. As a further comparison, Figure 10 reports the S_{11} parameter of the antenna simulated when a spherical post-ablation zone is placed at the center of phantom, 10 mm beneath the muscle-liver interface. The diameter of the ablation zone is 25 mm and its properties are $\epsilon_r = 26.67$, $\sigma = 1.26$ S/m [36]. As for the case of the 1-D analysis, we can notice that the presence of the ablation zone does not change the antenna matching as compared to the healthy liver case, confirming that the designed antenna is a suitable candidate for the MWI device. Moreover, a quantitative difference is observed in the S_{11} value in the band of interest (i.e., below 2 GHz). The inset in Figure 10 shows the corresponding differential signal, computed as the difference between the signals normalized to the amplitude of the healthy-liver signal. As can be noted, such a difference varies between -50 and -60 dB. Such a differential signal level is consistent with the 1-D analysis, which was referred to the power.

IV. Conclusion and Future Work

This study provides the initial guidelines on the frequency band, matching medium selection and antenna design, for the development of a microwave imaging device for monitoring thermal ablation treatments of liver tumors, by sensing the changes occurring in the treated tissue. The 0.5-2 GHz frequency band and a medium with permittivity equal to 23 have been identified as the suitable working conditions. With respect to those figures, three antipodal Vivaldi antennas were designed and numerically assessed. Once achieved the desired design, the presence of the SMA connector was simulated putting into evidence a matching issue determined by the difference in dielectric properties between the matching medium and antenna's substrate. To the best of our knowledge, this was the first time such an issue was evidenced; additionally, a simple and feasible solution was proposed. Future work includes the realization of the matching medium and AVA-RT antenna, to allow carrying out experiments for the proposed device. As a final comment, it is worth noting that, while the present study is referred to a device for monitoring thermal ablation of liver tissue, which is the most clinically relevant case, the methodology is general and can be applied for the design of devices for monitoring thermal treatments (ablation or hyperthermia) in regions of the body different from the liver.

References

[1] F. X. Bosch, J. Ribes, M. Dıáz, and R. Cléries, "Primary liver cancer: Worldwide incidence and trends," *Gastroenterol.*, vol. 127, no. 5, pp. S5–S16, 2004.

[2] B. Yang *et al.*, "Prospective study of early detection for primary liver cancer," *J. Cancer Res. Clin. Oncol.*, vol. 123, no. 6, pp. 357–360, 1997.

[3] C. J. Simon, D. E. Dupuy, and W. W. Mayo-Smith, "Microwave ablation: Principles and applications," *Radiographics*, vol. 25, pp. S69–S83, 2005.

[4] M. Ahmed and S. N. Goldberg, "Thermal ablation therapy for hepatocellular carcinoma," *J. Vasc. Interventional Radiol.*, vol. 13, no. 9, pp. S231–S243, 2002.

[5] B. Quesson, J. A. de Zwart, and C. T. Moonen, "Magnetic resonance temperature imaging for guidance of thermotherapy," *J. Magn. Reson. Imaging: Official J. Int. Soc. Magn. Reson. Med.*, vol. 12, no. 4, pp. 525–533, 2000.

[6] F. Liu, X. Yu, P. Liang, Z. Cheng, Z. Han, and B. Dong, "Contrast-enhanced ultrasound-guided microwave ablation for hepatocellular carcinoma inconspicuous on conventional ultrasound," *Int. J. Hyperthermia*, vol. 27, no. 6, pp. 555–562, 2011.

[7] S. N. Goldberg *et al.*, "Image-guided tumor ablation: Proposal for standardization of terms and reporting criteria," *Radiology*, vol. 228, no. 2, pp. 335–345, 2003.

[8] M. Ahmed *et al.*, "Image-guided tumor ablation: Standardization of terminology and reporting criteria a 10-year update," *Radiology*, vol. 273, no. 1, pp. 241–260, 2014.

[9] M. E. Abdelsalam and K. Ahrar, "Ablation of small renal masses," *Techn. Vasc. Interventional Radiol.*, p. 100674, 2020.
[10] P. Bruners *et al.*, "Ct-based temperature monitoring during hepatic RF ablation: Feasibility in an animal model," *Int. J. Hyperthermia*, vol. 28, no. 1, pp. 55–61, 2012.
[11] L. Shi and S. Tashiro, "Estimation of the effects of medical diagnostic radiation exposure based on DNA damage," *J. Radiat. Res.*, vol. 59, no. suppl$_2$, pp. ii121–ii129, 2018.
[12] H. Kuehl *et al.*, "Comparison of FDG-PET, PET/CT and MRI for follow-up of colorectal liver metastases treated with radiofrequency ablation: Initial results," *Eur. J. radiol.*, vol. 67, no. 2, pp. 362–371, 2008.
[13] M. Pastorino, *Microwave Imaging*. John Wiley and Sons, 2010, vol. 208.
[14] V. Lopresto, R. Pinto, and M. Cavagnaro, "Experimental characterisation of the thermal lesion induced by microwave ablation," *Int. J. Hyperthermia*, vol. 30, no. 2, pp. 110–118, 2014.
[15] R. Scapaticci, V. Lopresto, R. Pinto, M. Cavagnaro, and L. Crocco, "Monitoring thermal ablation via microwave tomography: An ex vivo experimental assessment," *Diagnostics*, vol. 8, no. 4, p. 81, 2018.
[16] J.-C. Bolomey and L. Jofre, "Three decades of active microwave imaging achievements, difficulties and future challenges," in *Proc. IEEE Int. Conf. Wirel. Inf. Technol. Syst*, 2010, pp. 1–4.
[17] E. Pittella, P. Bernardi, M. Cavagnaro, S. Pisa, and E. Piuzzi, "Design of UWB antennas to monitor cardiac activity," *ACES J.-Appl. Comput. Electromagnetics Soc.*, vol. 26, no. 4, p. 267, 2011.
[18] M. Abbak, M. Akıncı, M. Çayören, and İ. Akduman, "Experimental microwave imaging with a novel corrugated Vivaldi antenna," *IEEE Trans. Antennas Propagation*, vol. 65, no. 6, pp. 3302–3307, Jun. 2017.
[19] R. Scapaticci, M. Bjelogrlic, J. A. T. Vasquez, F. Vipiana, M. Mattes, and L. Crocco, "Microwave technology for brain imaging and monitoring: physical foundations, potential and limitations," in emerging electromagnetic technologies for brain diseases diagnostics, monitoring and therapy, L. Crocco, I. Karanasiou, M. L. James, and R. C. Conceição, Eds. Berlin, Germany: Springer, 2018, pp. 7–35.
[20] J. Bourqui, M. Okoniewski, and E. C. Fear, "Balanced antipodal Vivaldi antenna with dielectric director for near-field microwave imaging," *IEEE Trans. Antennas Propag.*, vol. 58, no. 7, pp. 2318–2326, Jul. 2010.
[21] I. Merunka, O. Fiser, L. Vojackova, J. Vrba, and D. Vrba, "Utilization potential of balanced antipodal Vivaldi antenna for microwave hyperthermia treatment of breast cancer," in *Proc. 8th Eur. Conf. Antennas and Propag.* (EuCAP 2014)., 2014, pp. 706–710.
[22] N. K. Nikolova, "Microwave imaging for breast cancer," *IEEE Microwave Magazine*, vol. 12, no. 7, pp. 78–94, Dec. 2011.
[23] I. G. Zubal, C. R. Harrell, E. O. Smith, Z. Rattner, G. Gindi, and P. B. Hoffer, "Computerized three-dimensional segmented human anatomy," *Med. Physics*, vol. 21, no. 2, pp. 299–302, 1994.
[24] O. Akkus *et al.*, "Evaluation of skin and subcutaneous adipose tissue thickness for optimal insulin injection," *J. Diabetes Metab*, vol. 3, no. 8, p. 2, 2012.
[25] S. Gabriel, R. Lau, and C. Gabriel, "The dielectric properties of biological tissues: III. parametric models for the dielectric spectrum of tissues," *Phys. Med. & biol.*, vol. 41, no. 11, p. 2271, 1996.
[26] C. A. Balanis, *Advanced Engineering Electromagnetics*. John Wiley and Sons, 1999.
[27] O. M. Bucci, L. Crocco, R. Scapaticci, and G. Bellizzi, "On the design of phased arrays for medical applications," *Proc. IEEE IRE*, vol. 104, no. 3, pp. 633–648, 2016.
[28] A. Abbosh, H. Kan, and M. Bialkowski, "Compact ultra-wideband planar tapered slot antenna for use in a microwave imaging system," *Microw. Optical technol. Letters*, vol. 48, no. 11, pp. 2212–2216, 2006.
[29] A. Molaei, A. G. Dagheyan, J. H. Juesas, and J. Martinez-Lorenzo, "Miniaturized UWB antipodal Vivaldi antenna for a mechatronic breast cancer imaging system," in *Proc. IEEE Int. Symp. Antennas and Propag. & USNC/URSI Nat. Radio Sci. Meeting*, 2015, pp. 352–353.
[30] B. M. Kolundžija and A. R. Djordjević, *Electromagnetic Modeling of Composite Metallic and Dielectric Structures*. Artech House, 2002.
[31] D. B. Davidson, *Computational Electromagnetics for RF and Microwave Engineering*. New York, NY, USA: Cambridge University Press, 2010.
[32] J. Van der Kruk, C. Steelman, A. Endres, and H. Vereecken, "Dispersion inversion of electromagnetic pulse propagation within freezing and thawing soil waveguides," *Geophysical Res. Lett.*, vol. 36, no. 18, 2009.
[33] J. Stang, M. Haynes, P. Carson, and M. Moghaddam, "A preclinical system prototype for focused microwave thermal therapy of the breast," *IEEE Trans. Biomed. Eng.*, vol. 59, no. 9, pp. 2431–2438, Sept. 2012.
[34] G. Ruvio *et al.*, "Comparison of coaxial open-ended probe based dielectric measurements on ex-vivo thermally ablated liver tissue," in *Proc. 13th Eur. Conf. Antennas and Propag.*, 2019, pp. 1–4.
[35] T. Maleszka and G. Jaworski, "Broadband stripline to microstrip transition with constant impedance field matching section for applications in multilayer planar technologies," in *Proc. 18-th Int. Conf. Microw., Radar and Wirel. Commun.*, 2010, pp. 1–4.
[36] V. Lopresto, R. Pinto, G. A. Lovisolo, and M. Cavagnaro, "Changes in the dielectric properties of ex vivo bovine liver during microwave thermal ablation at 2.45 GHz," *Phys. Med. & Biol.*, vol. 57, no. 8, p. 2309, 2012.

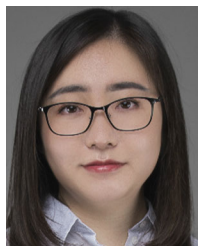

Mengchu Wang (Student Member, IEEE) received the B.Sc. degree in electrical engineering from the Nanjing University of Science and Technology, China, in 2011, and the M.Sc. degree in telecommunication from the Delft University of Science and Technology, the Netherlands, in 2015. She is currently working toward the Ph.D. degree with the Institute for Electromagnetic Sensing of the Environment, Naples, and Sapienza University of Rome. She worked as an RF Engineer with the Space Industry from 2016 to 2018. Her research activities are devoted to the development of the electromagnetic device for non-invasive monitoring of ablation treatments. She is an Early Stage Researcher of the project "EMERALD" which is in frame work of the European Union Horizon 2020 Research and Innovation Programme under the Marie Skłodowska-Curie Actions.

Lorenzo Crocco (Senior Member, IEEE) is a Research Director with the Institute for the Electromagnetic Sensing of the Environment, National Research Council of Italy (IREA-CNR). His scientific activities mainly concern of electromagnetic scattering, with a focus on diagnostic and therapeutic uses of EM fields, through-the-wall radar and GPR. On these topics, he has authored or coauthored more than 120 papers, given keynote talks and led or participated to research projects. Dr. Crocco is an Associate Editor for the IEEE JOURNAL OF ELECTROMAGNETICS, RF AND MICROWAVES IN MEDICINE AND BIOLOGY (IEEE J-ERM) and has edited a book on *Electromagnetic Technologies for Brain Diseases Diagnostics, Monitoring and Therapy*. From 2013, he is Italian representative in the Management Committees of COST actions devoted to medical applications of EM fields (MiMed on microwave imaging and MyWAVE on therapeutic applications of electromagnetic waves). Since 2017, he is member of the Board of Directors of the Italian Electromagnetic Society (SIEm). In 2018, he received the Full Professor habilitation in electromagnetic fields by the Italian Ministry of Research and University. Since 2019, he is a member of the Italian URSI Commission. In 2019, he has been elected in the Scientific Board of the Engineering Department (DIITET) of CNR. He was the recipient of the SIEm "Barzilai" Award for Young Scientists (2004) and YSA at the URSI General Assembly held in New Delhi (India) in 2005.

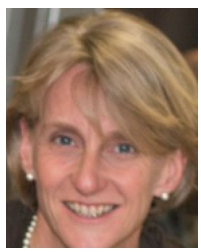

Marta Cavagnaro (Member, IEEE) received the Electronic Engineering degree (*cum laude*) and the Ph.D. degree in electronic engineering from the Sapienza University of Rome, Rome, Italy.

She is an Associate Professor with the Department of Information Engineering, Electronics and Telecommunications with the Sapienza University of Rome. She has authored or coauthored more than 200 scientific papers. Her research interests include related to dosimetric aspects of the interaction between electromagnetic fields and biological systems, medical applications, environmental impact of mobile communication systems, measurements of dielectric properties of tissues, and numerical techniques in electromagnetics.

Prof. Cavagnaro is an Associate Editor for the *Bioelectromagnetics journal*, and serves as anonymous reviewer for several scientific journals.